Iranian Journal of Oil & Gas Science and Technology, Vol. 9 (2020), No. 1, pp. 47-67
http://ijogst.put.ac.ir

Nitrogen Adsorption on Molecular Sieve Zeolites: An Experimental and Modeling Study

Erfan Touraji and Ahad Ghaemi*

[1] M.S. Student, School of Chemical, Petroleum, and Gas Engineering, Iran University of Science and Technology, P.O. Box 16846-13114, Tehran, Iran

[2] Associate Professor, School of Chemical, Petroleum, and Gas Engineering, Iran University of Science and Technology, P.O. Box 16846-13114, Tehran, Iran

Received: June 04, 2019; *revised*: October 17, 2019; *accepted*: November 03, 2019

Abstract

Separation of nitrogen from a gaseous mixture is required for many industrial processes. In this study, the adsorption of nitrogen on zeolite 4A was investigated in terms of different adsorption isotherm models and kinetics. An increase in the initial pressure from 1 to 9 bar increases the amount of adsorbed nitrogen from 6.730 to 376.030 mg/(g adsorbent). The amount of adsorbed nitrogen increased from 7.321 to 40.594 mg/(g adsorbent) by raising the temperature from 298 to 333 K at a pressure equal to one bar; however, it then dropped to 15.767 mg/(g adsorbent) when temperature decreased to 353 K. Increasing the amount of the adsorbent from 1 to 4 g decreased the specific adsorption from 67.565 to 21.008 mg/(g adsorbent) at a temperature of 298 K and a pressure of 3 bar. Furthermore, it was found that the nitrogen adsorption experimental equilibrium data are consistent with Sips and Langmuir-Freundlich models. The highest overlap was achieved through second order and Ritchie's models.

Keywords: Adsorption, Nitrogen, Molecular Sieve, Isotherm, Kinetics

1. Introduction

Nitrogen is one of the most active elements in the planet, and its separation as an inert gas plays an important role in engineering processes. Oil includes a large amount of nitrogen and sulfur compounds, which are considered as air pollutants (Ahmadi et al., 2019). Some fuels which include nitrogen result in NOx emissions in internal combustion engines (Rashidi et al., 2015). Furthermore, adsorption is more easily performed in a gas phase than a liquid phase (Hajilari et al., 2019). In addition, zeolite has been reported by many researchers as a suitable adsorbent for adsorption processes (Ahmadpour et al., 2018; Khajeh Amiri et al., 2019). Accurate adsorption equilibrium data are necessary to simulate and design a pressure swing adsorption process for separating nitrogen from other gases and vapors. In processes of fixed bed gas adsorption, equilibrium capacity, equilibrium pressure, equilibrium temperature, and so on are the significant parameters and valuable indices for measuring the adsorption capacity (Aroua et al., 2008; Mahdizadeh and Ghaemi, 2019). The

* Corresponding author:
Email: aghaemi@iust.ac.ir

enhancement of a utilitarian adsorbent for methane separation allows the economic extraction of natural gas sources remained unexploited because of their high nitrogen contents (Dolan and Butwell, 2002). Tanaka et al. reported that nitrogen is useful for the packaging of medicines in the pharmaceutical industry because nitrogen operates as a protective gas in the package and prevents the drug from oxidation and/or degradation (Tanaka et al., 1987). As a result, having accurate data for the adsorption of nitrogen over a wide range of pressures and temperatures in various molecular sieves is of great importance.

Zeolites 4A, as a strong solid, have pores with the same size of nitrogen molecules (Smith and Klosek, 2001; Bayati et al., 2016). Thus, zeolites are expected to be useful for the selective separation of nitrogen from gaseous mixtures. The non-regular electric fields available in the void spaces of zeolites can cause the preferential adsorption of molecules which are more polarizable. In addition to the equilibrium capacity of the zeolites to adsorb N_2, the mass transfer dynamics is of great importance to the design of separation units. An adsorption process usually involves three transmission processes for the absorbing materials:

- Transferring from the absorbing mass to the layer in the domain of absorbent;
- Transferring from the layer to the absorbent surface;
- Transferring from the surface layer to the internal sites and then connecting to effectual sites.

However, in the kinetic modeling, all the three main stages can work together, and it is supposed that the precise difference between the mean equilibrium concentration and the mean concentration of the solid phase (stage) can be taken into consideration as the driving force of adsorption (Mirzaei and Ghaemi). Additionally, according to experimental observations at an optimal stirring speed, external conditions have a very little effect (Cussler, 2009).

Mendes and Costa presented a simulation study using a pressure swing adsorption (PSA) as an equilibrium-based component separation process by running Skarstrom cycle. Their work was based on the experimental results obtained for the separation of oxygen from the air using zeolite 5A (Mendes et al., 2000). Fernandez et al. studied the theoretical analysis of the separation of oxygen and nitrogen in the air by a PSA separation process (Fernandez, 1983). In another study, Hassan and Ruthven developed a dynamic model for a PSA separation process which was expanded based on the linearized mass transfer rate (Hassan et al., 1986). Farooq et al. derived a numerical model to simulate the equilibrium separation of air in a zeolite PSA unit (Farooq et al., 1989). They also studied the linear mass transfer model with frozen solid approximation during pressurization (Farooq et al., 1990). In addition, a micropore diffusion model was developed for a binary bulk PSA gas separation process according to Langmuir equilibrium (Farooq and Ruthven, 1991). Budner et al. studied an isothermal and non-equilibrium mathematical model derived for the multicomponent adsorption (Budner et al., 1999). Cruz et al. reported an innovative method to optimize the cyclic adsorption separation processes (Cruz et al., 2005). Moghadazadeh et al. worked on the experimentation and modeling of a four-bed PSA process in a zeolite 13X to obtain oxygen-enriched air (Moghadazadeh and Mofarahi, 2008). In general, Table 1 summarizes the experimental conditions of the studies conducted on nitrogen adsorption.

Table 1

Reported values of nitrogen adsorption on different adsorbents.

Author	*T* (K)	*P* (bar)	Adsorbent	Year
Mendes et al.	293.15	3-7.1	Zeolite (5A)	2000

Author	*T* (K)	*P* (bar)	Adsorbent	Year
Mendes et al.	293.15	4.2	Zeolite (5A)	2001
Fernandez et al.	300	6	Carbon Active	1983
Hassan et al.	298.15	3	Zeolite (5A)	1986
Farooq et al.	298.15	1	Zeolite	1989
Farooq et al.	300	6/1	Zeolite (4A)	1990
Farooq et al.	298.15	3	Zeolite (5A)	1991
Budner et al.	293.15	0.2-1.5	Zeolite (5A&13X)	1999
Cruz et al.	293.15	3	Zeolite (5A&13X)	2005
Moghadazadeh et al.	293.15-300.15	3.5-6.5	Zeolite (13X)	2008

This study presents the kinetic parameters and provides new insights into the mechanism of the adsorption of nitrogen by molecular sieve zeolites. The effects of operating parameters such as pressure, temperature, and the amount of adsorbent on the adsorption of nitrogen are also scrutinized. However, it should be noted that the current work is limited to the process of pure nitrogen adsorption and does not seek to address the selectivity of adsorption.

2. Materials and methods

2.1. Materials

Purified nitrogen (99.99%) was supplied by Hamta gas, and the synthetic molecular sieve was manufactured by Nitel Pars under the trade name of Molecular Sieves Type 4A. It is granular in the spherical form of HYG04B (3-5 mm), and its average density is 0.72 g/ml. Figure 1 displays the structure of zeolite A.

a) b)

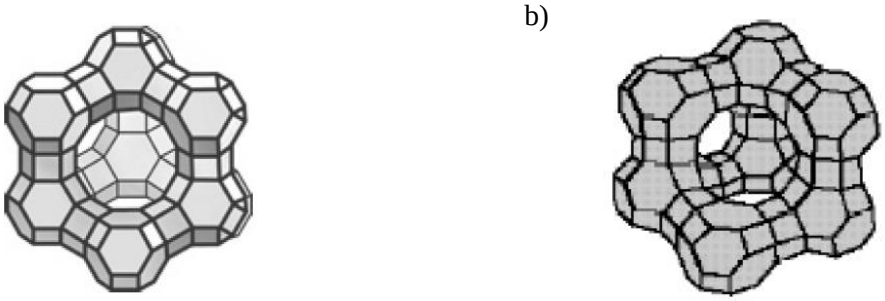

Figure 1

a) Structure of zeolite A and b) structure of X zeolites.

Table 2 tabulates the analysis of the surface area and average pore size of the adsorbent.

Table 2

Characteristics of zeolite molecular sieve as provided by the manufacturer.

Specification	Water adsorption 50% relative humidity & at 298 K (wt.%)	Attrition (wt.%)	Density (g/ml)	Crush (N)	Moisture content (wt.%)
Bead 4A (3.0-5.0 mm)	22.50	0.01	0.76	90.00	0.60

The structure and properties of the adsorbent affect the creation of strong interactions between the adsorbent and nitrogen gas in the process of adsorption. In this context, the attrition and pore size of the adsorbent are the important factors influencing the amount of N_2 adsorbed at equilibrium. In fact, the pore size of the adsorbent must match the size of nitrogen molecules (i.e., 3.8 angstroms). Therefore, the zeolite molecular sieve 4A used herein is expected to be suitable for the adsorption of nitrogen.

The Fourier transform infrared (FTIR) was employed in order to identify the bonds and the chemical structure of the solid and liquid samples, particularly zeolite 4A. The FTIR spectrometer used in this work is VERTEX 70v FTIR Spectrometer by Bruker. According to the FTIR spectra of zeolite 4A (Figure 2), the typical peaks of zeolite 4A appear in the wave number range of 3300-3600 cm^{-1}.

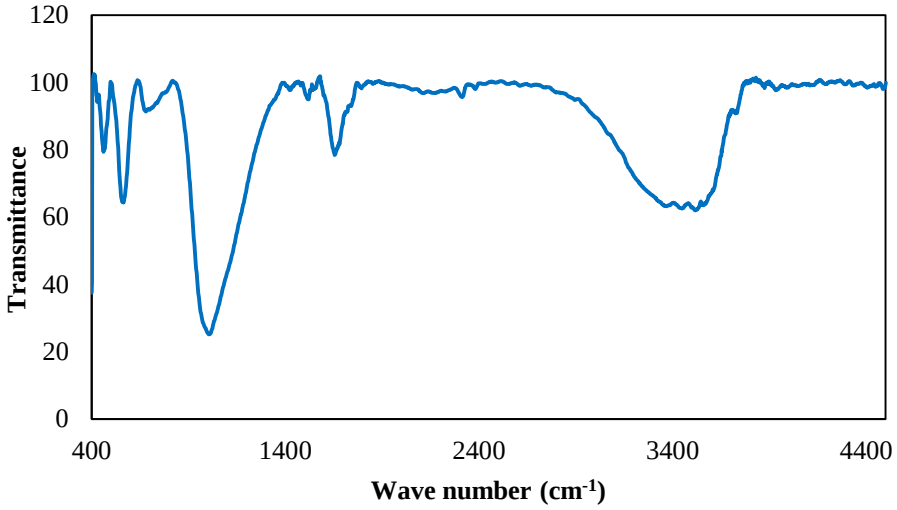

Figure 2

FTIR spectra of zeolite 4A.

To investigate the morphology of zeolite 4A powder in a solid state, Siemens D 5000 powder X-ray diffractometer was employed. Figure 3 delineates the XRD diffraction spectra of zeolite 4A and shows that no other phase can be observed for zeolite powder. CuKα source leads to the development of X-rays with a wavelength of 1.5406 Å. The extent of diffraction, i.e. the degree of 2θ, was varied from 5 to 80° to discern any fluctuations in the morphological features of the crystals and the intermolecular gap between inter-segmental connections after crosslinking.

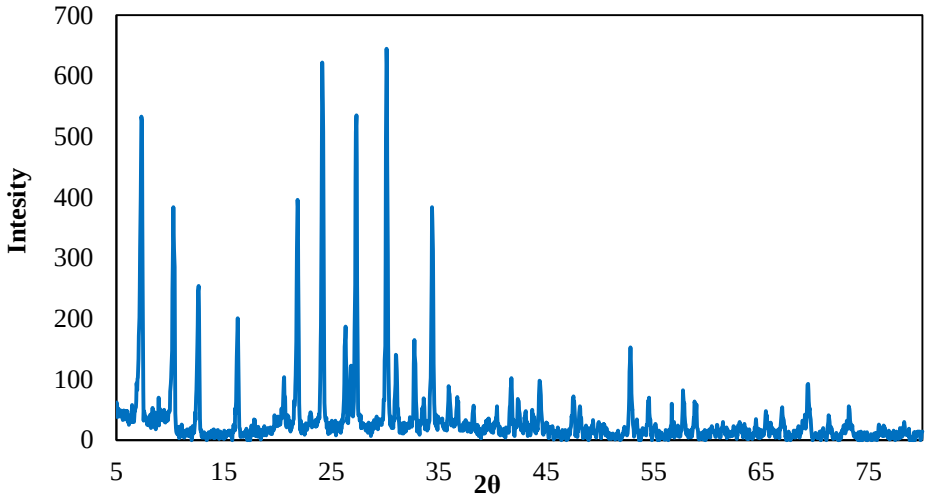

Figure 3

XRD patterns of zeolite 4A.

2.2. Adsorption apparatus

An overview of the adsorption process is illustrated in Figure 4. Nitrogen adsorption capacity is measured using zeolite 4A solid adsorbent. After being weighed by a digital scale, the molecular sieve was transferred into a batch stainless steel reactor. The length, inner radius, and internal volume of the reactor is 9 cm, 3 cm, and 254.34 cm^3 respectively. After setting the temperature and pressure of the reactor, nitrogen was added to the reactor. The temperature and pressure of the reactor were measured and monitored to two decimal places per second. After one hour, all the data, including temperature (K), pressure (bar), date, and time (second) were stored in Microsoft Excel format. Finally, the density of nitrogen adsorbed was calculated with pressure. In addition, the adsorption capacity of the adsorbent was calculated using the below equation (Saeidi et al., 2018):

$$q_e = \frac{\left(P_{N_2}^{initial} - P_{N_2}^{final}\right) V M_{N_2}}{RTm} \times 1000 \quad (1)$$

$$k_d = \frac{P_{N_2}^{initial} - P_{N_2}^{final}}{P_{N_2}^{final}} \frac{V}{W} \left(\frac{cm^3}{g}\right) \quad (2)$$

where, q_e (mg/g) is the adsorption magnitude, and W is the weight of the adsorbent; V stands for the volume of the gas; k_d is distribution coefficient; $P_{N_2}^{initial}$ (bar), $P_{N_2}^{final}$ (bar), and m (g) represent the initial pressure of nitrogen, the final pressure of nitrogen, and the mass of the adsorbent respectively

To investigate a process of trial and error, a nonlinear method was run. In fact, a decrease in the error procedures is seen, when the coefficient of determining gap between the predicted data and experimental data (R^2) reaches the least amount; this process takes advantage of a solver add-in in Microsoft Excel (Li and Hitch, 2015). To analyze the effectuality of the experimental data in the isotherm models, nonlinear R^2 was used as a quantitative procedure. Moreover, the percentage of nitrogen adsorption was figured by the following equation (Wang and Bricker, 1979):

$$Adsorption(\%) = \frac{P_{N_2}^{initial} - P_{N_2}^{final}}{P_{N_2}^{initial}} \times 100 \quad (3)$$

where, $P_{N_2}^{initial}$ and $P_{N_2}^{final}$ represent the primary concentration and the equilibrium concentration of nitrogen respectively (Khajeh and Ghaemi, 2020).

$$R = \frac{N\sum XY - \left(\sum X\right)\left(\sum Y\right)}{\left[N\sum X^2 - \sum X^2\right]\left[Ny^2 - y^2\right]} \quad (4)$$

where, N is the number of the data, and $\sum xy$ represents the sum of the multiplication of x, the experimental data, and y, the estimates of the data by the isotherm curve; $\sum x$ is the sum of the experimental data, and $\sum y$ denotes the sum of the data estimated by the isotherm curve. The average absolute value of relative error (AARE) is utilized to compare the predicted results with the experimental data as follows (Rahmati et al., 2012):

$$AARE = \frac{1}{N}\sum_{i=1}^{N}\left|\frac{\text{Predicted value} - \text{Experimental value}}{\text{Experimental value}}\right| \quad (5)$$

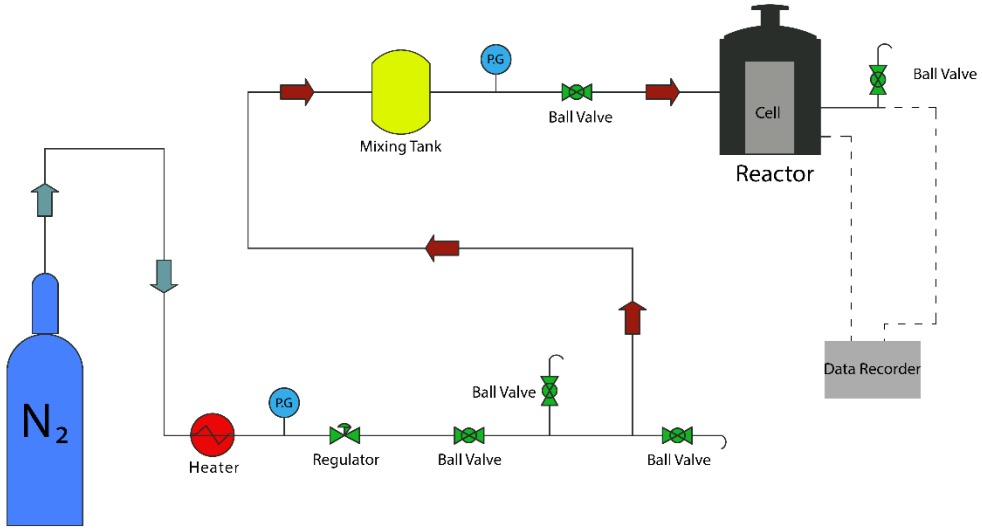

Figure 4

A schematic of adsorption setup.

2.3. Experiments

The adsorption equilibrium was achieved in a closed system. The adsorbent was weighed with a digital scale and placed in the reactor, and the reactor was then closed. Afterward, the nitrogen cylinder valve was opened, and nitrogen after passing a regulator, which sets the desired pressure of nitrogen, flows to a middle tank to reach the desired temperature; the adsorbent was also heated to reach the desired temperature. Next, the ball valve was opened to allow nitrogen into the molecular sieve chamber. The experiment was stopped after one hour. Temperature is controlled by a heater and

monitored by a personal computer, and the equilibrium data corresponding to each temperature are stored.

3. Results and discussion

3.1. Isotherm modeling

It is necessary to derive theoretical isotherms based on various physical models and to compare them with isotherms observed experimentally so as to develop a particular model which is valid under the given experimental conditions (Elshishini and Elnashaie, 1994). Among the predominated models, the Langmuir adsorption model is the easiest method to explain the adsorption onto the adsorbent layer, and there are equal energetic numbers of the adsorption parts. The Langmuir model is presented by Equation 6 as follows:

$$q_e = \frac{q_m K_L P_{N_2}}{1 + K_L P_{N_2}} \tag{6}$$

where, q_e (mg/g) is the quantity of N_2 adsorbed at equilibrium, and q_m (mg/g) denotes the maximum adsorption capacity of the adsorbent; P_{N_2} (bar) represents the balanced pressure of the gas adsorbed, and K_L (1/bar) stands for the Langmuir adsorption constant which is related to the free adsorption energy (Li and Hitch, 2015). The Freundlich isotherm framework is one of the earliest known correlations which can represent a reversible and nonideal adsorption process (Chen, 2015). Compared with the Langmuir model, the Freundlich adsorption isotherm, which is based on the idea that the adsorption energy exponentially decreases with the pressure of the adsorption process, can also be applied to the multilayer adsorption (Fil et al., 2012). Equation 7 expresses the Freundlich isotherm (Li and Hitch, 2015):

$$q_e = k_1 \times P_{N_2}^{\frac{1}{n}} \tag{7}$$

where, n and k_1 (g.bar/mmol) represent the coefficient and the constant of the Freundlich isotherm respectively. When the value of k_1 increases, the adsorption capacity of adsorbent for a presented adsorbate improves. The Langmuir-Freundlich (LF) isotherm demonstrates the correlation between the stability in heterogeneous systems using three fitting coefficients: N_t, m, and a. Both Freundlich and Langmuir isotherms have two main parameters. However, Langmuir-Freundlich isotherm is a three-parameter model, in which $v = \theta v_{m,}$ and v_m is an adjunct constant. The Langmuir-Freundlich equation (Equation 8) is suitable for obtaining the relationship between data when pressure and temperature greatly vary and the Langmuir and Freundlich isotherms are not able to adopt a relation (Yang, 2013; Umpleby et al., 2001):

$$\frac{P}{V(P_0 - P)} = \frac{1}{V_m C} + \frac{C-1}{V_m C}\left(\frac{P}{P_0}\right) \tag{8}$$

The model of Sips isotherm integrates the Freundlich and Langmuir isotherms, and the difference between the Sips isotherm and the Langmuir model stems from an adjunct parameter, namely n, which is defined as the system heterogeneity (Delavari Amrei et al., 2008). The Sips isotherm model is given by Equation 9:

$$q_e = \frac{K_s P_{N_2}^{\beta_s}}{1 - a_s P_{N_2}^{\beta_s}} \tag{9}$$

where P_{N2} is the pressure in bar, and K_s (Lg^{-1}) stands for Sips isotherm model constant; β_s is a dimensionless parameter that qualitatively characterizes the heterogeneity of the adsorbate-adsorbent system, and a_s (Lg^{-1})is Sips isotherm model constant.

The isotherm of Koble-Corrigan is a three-parameter equation which combines both the Langmuir and Freundlich isotherm frameworks to indicate the stability of the adsorption data. The Koble-Corrigan isotherm model is defined by Equation 10 (Koble and Corrigan, 1952):

$$q_e = A \times \frac{P_{N_2}^n}{\left(1 + B \times P_{N_2}^n\right)} \tag{10}$$

By using a trial-and-error optimization, the isotherm constants, including *A*, *B*, and *n* are calculated by means of a linear plot. Compared with linearized methods, the nonlinear method is the best approach to obtaining the isotherm parameters. Consequently, a nonlinear method should be adopted to determine the isotherm parameters.

On the other hand, to investigate trial-and-error procedures a nonlinear method is employed. In order to compare the usefulness of predominated isotherm models in fitting the experimental data, nonlinear R^2 was implemented. The parameters of the calculated isotherm models are listed in Table 3. Also, it should be mentioned that, in the current work, a nonlinear method is preferred to calculate the isotherm parameters. Figure 5 depicts the difference between the different isotherm models fitting the experimental data.

Table 3

The calculated parameters of isotherms models

Model	Parameter	Value	R^2	AARE
		Two-parameter models		
Langmuir	q_m	1232.473	0.977	1.341
	K_L	0.050		
Freundlich	k_1	56.990	0.9656	1.752
	N	1.108		
		Three-parameter models		
Langmuir-Freundlich	q_m	316.218	0.999	0.213
	K	0.005		
	n	0.058		
Sips	K_s	18.188	0.999	0.213
	β_s	2.724		
	a_s	0.058		
Koble-Corrigan	A	18.187	0.999	0.213
	n	2.785		
	B	0.058		

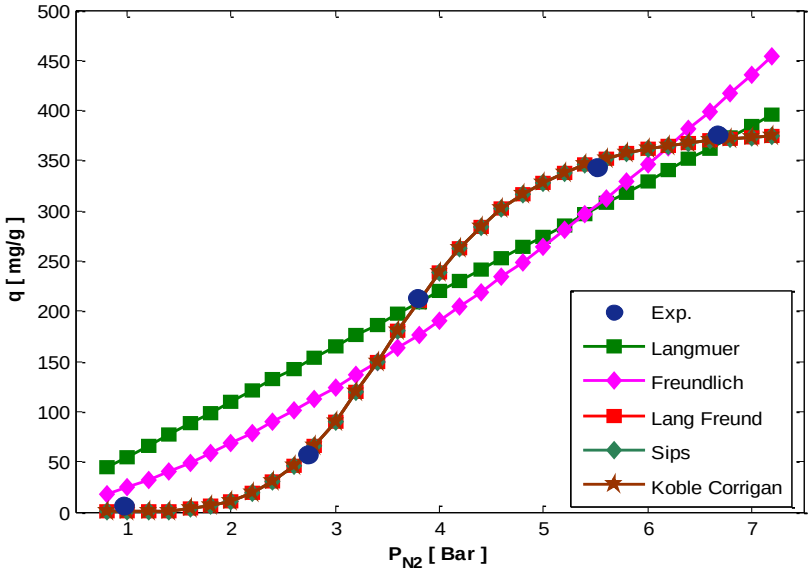

Figure 5

Different isotherm models fitting experimental data on N_2 adsorption on zeolite 4A at a temperature of 298 K and at pressures of 1, 3, 5, and 7 bar.

The investigation of isotherm elements indicates that finding the best model fitting the experimental data is one of the main analyses to explain the adsorption process mathematically. To figure out the features of the adsorbent, experimental steady data on nitrogen adsorption were fitted by the models introduced by scholars such as Langmuir-Freundlich, Hill, Redlich Peterson, Sips, Koble-Corrigan, and Radke Prausnitz Khan. The isotherm parameters of these models for a nitrogen adsorption process on zeolite at a temperature of 298 K and pressures of 1, 3, 5, and 7 bar are tabulated in Table 4. Arguably, the isotherm models developed by Sips, Koble-Corrigan, and Langmuir-Freundlich consider the chemical reactions between zeolite and N_2 (Langmuir, 1916).

Table 4

List of various adsorption kinetic models.

Kinetics model	Nonlinear equations	References
First order	$q_t = q_e\left(1-\exp\left(-k_1 t\right)\right)$	(Subha and Namasivayam, 2008)
Second order	$q_t = k_2 q_e^2 \dfrac{t}{\left(1+k_2 q_e t\right)}$	(Subha and Namasivayam, 2008)
Elovich equation	$q_t = \beta\log\left(\alpha a\beta\right)+\beta\log\left(t\right)$	(Low, 1960)
Ritchie second order	$q_t = q_e - \dfrac{q_e}{\left(1+K_2 t\right)}$	(Low, 1960)
Rate controlling	$q_t = k_{id} t^{0.5}$	(Ho, 2006)

3.2. Kinetic modeling

Mass transfer kinetics is a general term associated with resistance to mass transfer within particles. In order to explore the kinetics of nitrogen adsorption on solid adsorbents, kinetic equations of the adsorption processes controlling mechanisms such as diffusion and adsorption in the molecular layer of chemicals are used. Kinetic models were assessed to match the experimental data which were measured by first order, second order, Ritchie's second order, Elovich, and rate controlling kinetic equations.

Based on the theoretical perspectives, the first-order models are satisfactory when the adsorption on an adsorbent layer is low, and the adsorption mass reaches the highest degree. When the concentration of an adsorbate on an adsorbent is high, and the adsorption mass does not reach an equilibrium (Qiu et al., 2009), the second-order models are more suitable. Thus, it can be stated that a second-order model is useful for exploring the rate of the dependency of adsorption on the sorption scope of a certain layer (Subha and Namasivayam, 2008). Chemisorption kinetic equation was developed by Zeldowitsch (1934). It was then exploited to explain the rate of the adsorption of carbon monoxide on manganese dioxide, which diminishes exponentially with an increase in the quantity of gas adsorbed, and named Elovich equation (Low, 1960). The critical perspective of the Ritchie second-order model is that one adsorbate can be adsorbed onto the sites of two layers; as a result, a chemical equation is derived (Cheung et al., 2001). The adsorption process on permeable solids can be divided into three major steps: (1) mass transfer (boundary layer/film diffusion), (2) intra-particle diffusion, and (3) sorption of ions onto sites. In various cases, there is viability that intra-particle diffusion may be established as the rate-limiting stage, so it was introduced as the rate controlling model by Kathikeyen (2005) (Ho, 2006).

Fitting experimental data with the models based on adsorption kinetics is illustrated in Figure 6, and the parameters of the estimated kinetic models are listed in Table 5. As indicated in both Table 5 and Figure 6, small R^2 values of the pseudo-first-order models indicates that these models do not well match the experimental data, whereas the pseudo-second-order models with R^2 values close to unity well fit all the experimental results. Additionally, since our apparatus does not lag behind, the pressure responses are employed to measure kinetic uptake curves as also seen in previous studies of Saeidi et al. (2018) and Fashi et al. (2018).

Table 5

The values obtained for the parameters of different adsorption kinetic models at different temperatures.

Kinetic model	Parameter	T = 298.15 K	T = 313.15 K	T = 333.15 K	T = 353.15 K
Experimental	q_e	20.605	39.657	56.090	47.219
First order	q_e	19.994	40.435	54.970	48.289
	K_1	0.003	0.0572	0.016	0.048
	R^2	0.982	0.993	0.981	0.996
	AARE	0.174	0.084	0.458	0.342
	ARE				
Second order	q_e	22.925	41.004	56.994	48.898
	K_2	2×10-4	0.003	6×10-4	0.003
	R^2	0.991	0.990	0.997	0.990
	AARE	0.113	0.124	0.057	0.131

Kinetic model	Parameter	T = 298.15 K	T = 313.15 K	T = 333.15 K	T = 353.15 K
Ritchie second order	q_e	22.925	41.004	56.994	48.898
	k_2	0.004	0.127	0.033	0.133
	R^2	0.991	0.990	0.997	0.990
	AARE	0.162	0.176	0.043	0.142
Elovich	α	0.018	0.083	0.0763	0.129
	β	4.255	1.133	3.971	1.338
	R^2	0.987	0.581	0.918	0.0597
	AARE	0.235	1.445	0.654	5.687
Rate controlling	k_{id}	0.550	1.204	1.632	1.431
	R^2	0.944	0.501	0.693	0.439
	AARE	0.357	1.782	0.1653	2.135

According to R^2 values, the temperature difference between the best and worst models is chosen. Thus, at a temperature of 298 K, the second order and Ritchie second order models performed excellently, while the weakest model was the rate controlling model. Similarly, at a temperature of 353.15 K, the best and worst models are the second order and rate controlling models respectively. Generally, at all temperatures, the second order and Ritchie second order models suitably predicted the experimental data, which demonstrates that the adsorption of nitrogen follows a nonlinear model.

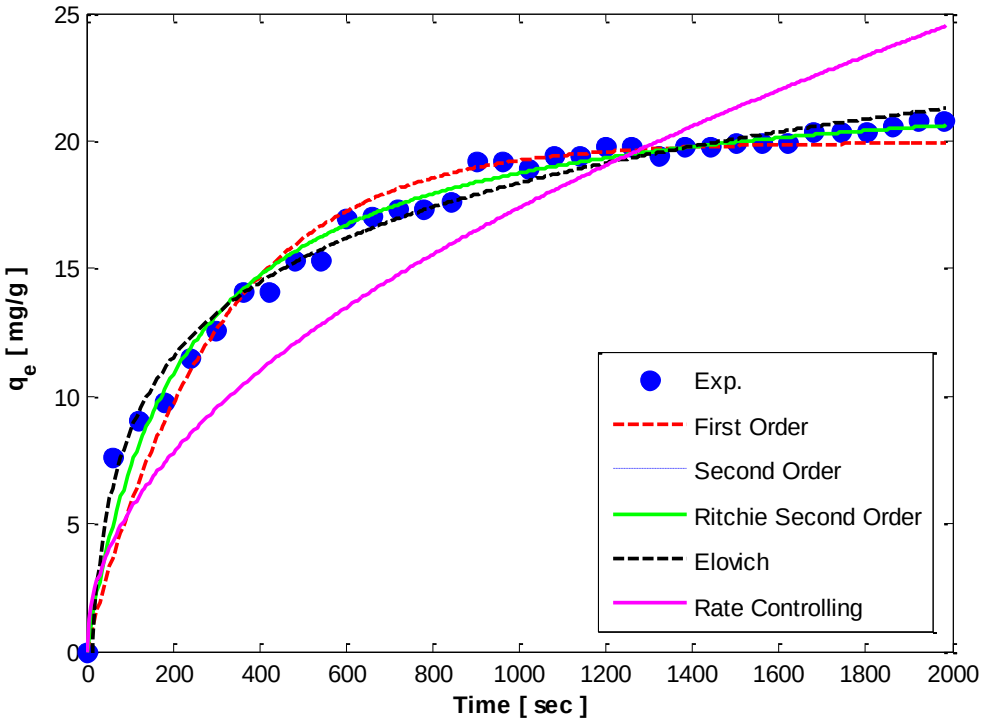

Figure 6

Experimental data and kinetic models of N_2 adsorption on zeolite 4A at a temperature of 298 K.

3.3. Adsorption thermodynamics

Gibbs free energy factors along with engineering practice entropy can be taken into account in order to explore what process happens spontaneously. The elements of thermodynamic such as the change in Gibbs free energy (ΔG°), enthalpy change (ΔH°), and entropy change (ΔS°) can be calculated by the use of variation of equilibrium with temperature. Therefore, the distribution coefficient is related to the enthalpy change (ΔH°) and entropy change (ΔS°) at a certain temperature as defined by the following equation:

$$\ln K_d = \frac{\Delta S^o}{R} - \frac{\Delta H^o}{RT} \tag{16}$$

where, K_d (cm^3/g) is the distribution coefficient, and ΔS° and ΔH° represent the standard entropy and standard enthalpy respectively; R (kJ/(mol.K)) stands for gas constant, and T (K) is the absolute temperature. The standard Gibbs free energy is estimated by using the following formula:

$$\Delta G^o = \Delta H^o - T\Delta S^o \tag{17}$$

The values of entropy change (ΔS°) and enthalpy change (ΔH°) are respectively estimated by the slope and y-intercept of the plot of ln (K_d) versus (1/T) (see Figure 7).

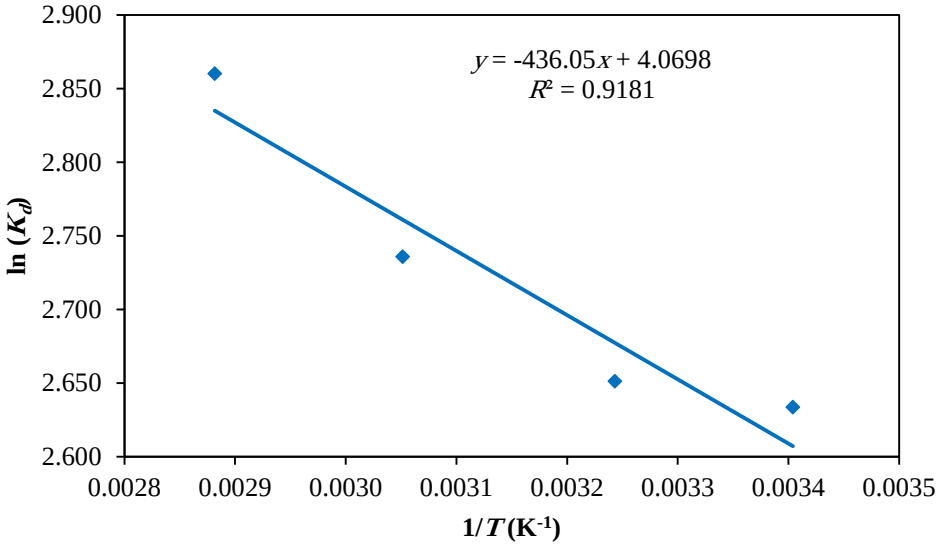

Figure 7

Relationship between ln(K_d) and 1/T for the adsorption of N_2 on zeolite 4A.

The Gibbs free energy at all the temperatures is negative, and a decrease in the value of ΔG° with an increase in temperature confirms that the adsorption is carried more easily at high temperatures. The percentage of variation in adsorption with temperature is displayed in Figure 8. Table 6 also summarizes the thermodynamic data relevant to this adsorption process.

Table 6

The obtained thermodynamic parameters.

P (N_2) (bar)	ΔH (kJ/mol)	ΔS (kJ/mole K)	ΔG (kJ/mol)			
			T = 298.15 K	T = 313.15 K	T = 333.15 K	T = 353.15 K

P **(N_2) (bar)**	**ΔH (kJ/mol)**	**ΔS (kJ/mole K)**	**ΔG (kJ/mol)**			
1.000	29.209	-0.080	53.096	54.298	55.900	57.50242
9.000	41.305	-0. 102	67.543	68.678	69.634	71.341

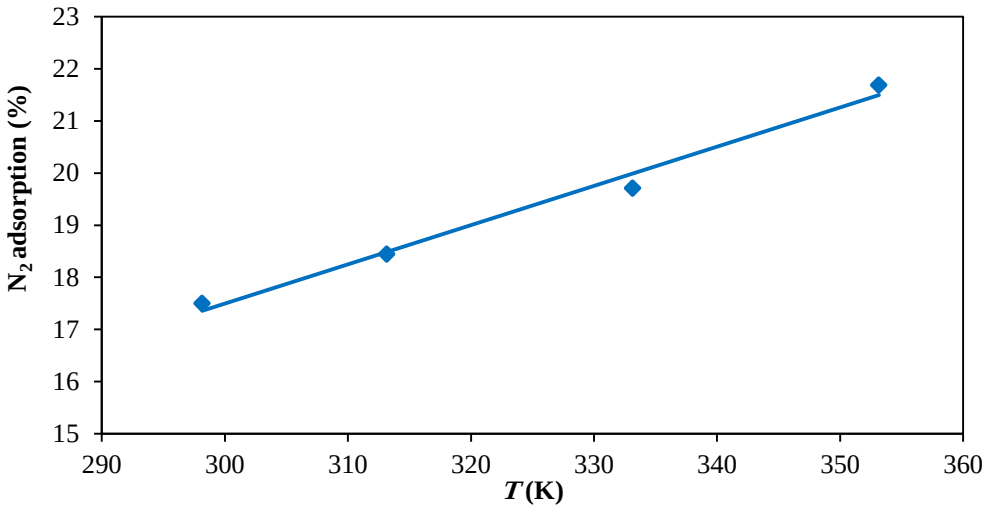

Figure 8

The variation of the percentage of N_2 adsorption on zeolite 4A with temperature.

3.4. Effect of the amount of adsorbent on adsorption capacity

The variation of the amount of nitrogen adsorbed as a function of time at different amounts of molecular sieve is illustrated in Figure 9. Four different amounts of molecular sieve adsorbents, namely 1, 2, 3, and 4 g, were selected for nitrogen adsorption. Figure 10 also delineates the capacity of nitrogen adsorption on zeolite 4A simultaneously as a function of the amount of adsorbent and time at a temperature of 298 K and at a pressure of 3 bar. Moreover, Figure 11 represents the effect of the amount of adsorbent on the amount of adsorbed nitrogen. It is clear that increasing the amount of adsorbent improves the adsorption capacity of nitrogen. Furthermore, although raising the amount of adsorbent increases the amount of absorbed gas, an increase in the amount of adsorbent reduces the ratio of adsorption to the amount of adsorbent. In this work, a pressure of 3 bar was selected for investigating the amount of adsorbent on the adsorption capacity because this pressure can more easily be controlled compared to a pressure of 6 or 9 bar; also, in comparison with a lower pressure of 1 bar, the difference in the adsorption capacity at a pressure of 3 bar can better be noticed. When the amount of adsorbent increases in reactor, the contact area between the adsorbent granules is increased, while the contact area between nitrogen and adsorbent particles is reduced, thereby decreasing the adsorption capacity.

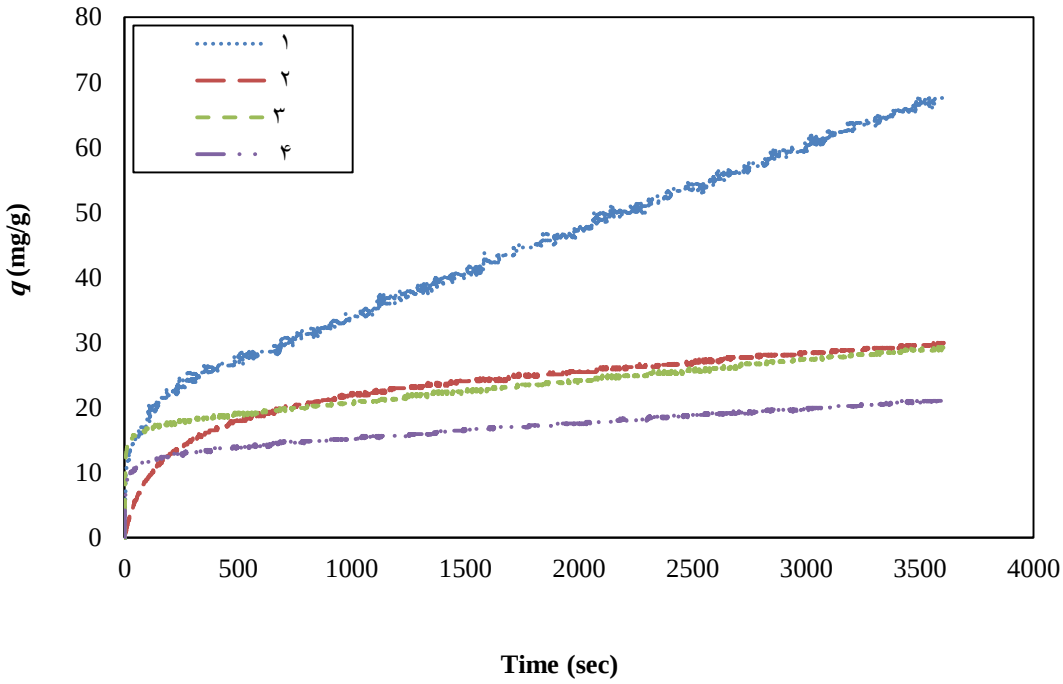

Figure 9

The variation of the amount of gas adsorbed on zeolite 4A as a function of time at a temperature of 298 K.

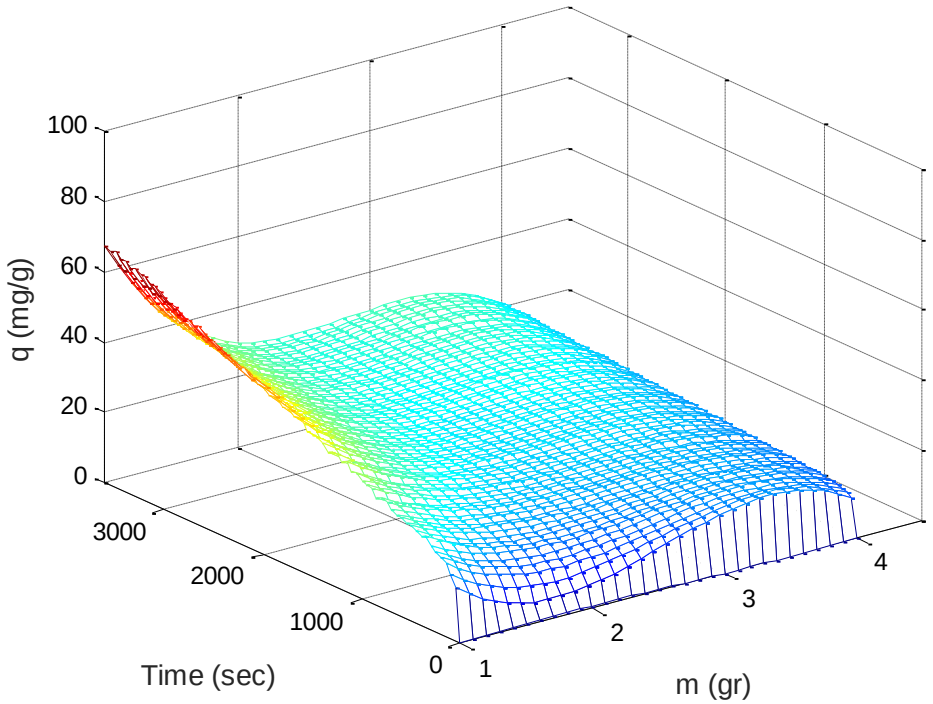

Figure 10

Three-dimensional display of the simultaneous effect of the amount of adsorbent and time on the capacity of nitrogen adsorption on zeolite 4A.

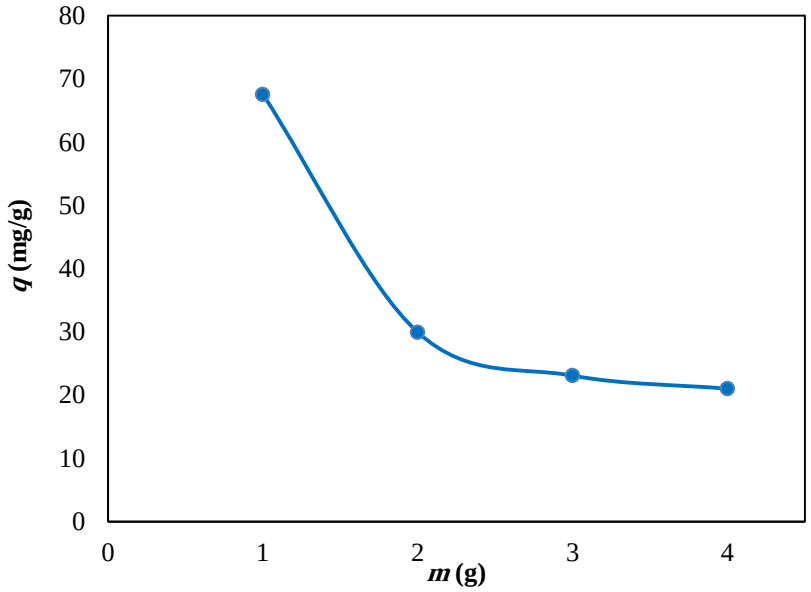

Figure 11

The effect of the amount of adsorbent on the amount of adsorbed nitrogen.

3.5. Effect of temperature on adsorption capacity

The effect of different adsorption temperatures, including 298.15, 313.15, 333.15, and 353.15 K on the variation of nitrogen adsorption on zeolite molecular sieve 4A with time is drawn in Figure 12. In addition, the variation in the percentage of N_2 adsorption as a function of temperature is depicted in Figure 13. Figure 14 also represents the simultaneous effect of temperature and time on the capacity of nitrogen adsorption. The nitrogen adsorption capacity at a pressure of 1 bar, at a temperature of 298.15 K, and after 3600 seconds is 7.321 mg/g, and it gradually increases to 40.594 mg/g at a temperature of 333.15 K and to 15.767 mg/g at a temperature of 353.15 K. The maximum capacity of nitrogen adsorption is obtained at a temperature near 333.15 K, which is selected as the optimum temperature of the adsorption process.

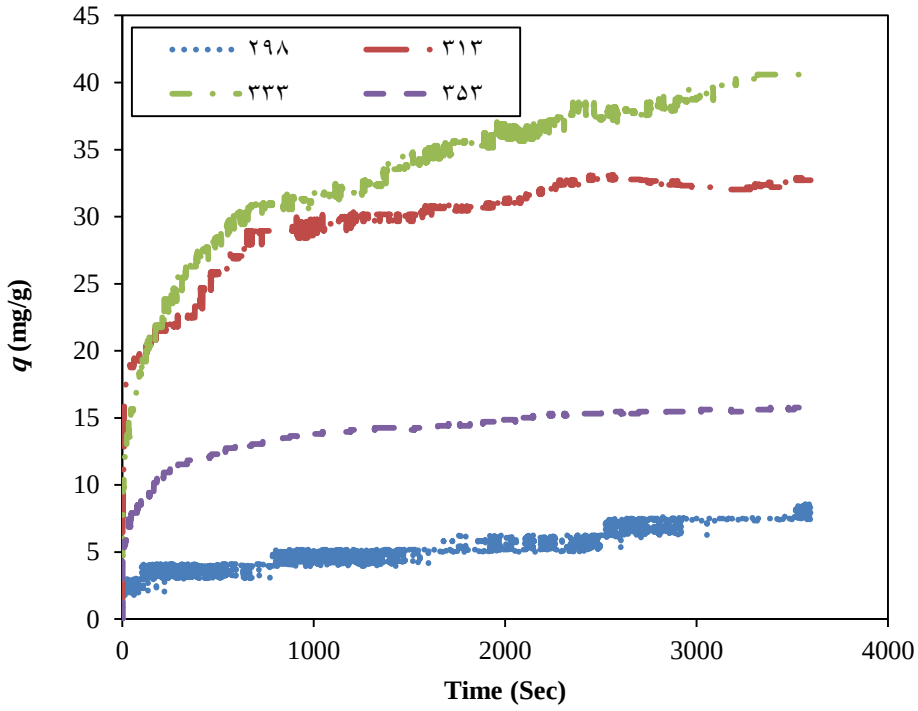

Figure 12

The variation of nitrogen adsorption with time at different temperatures.

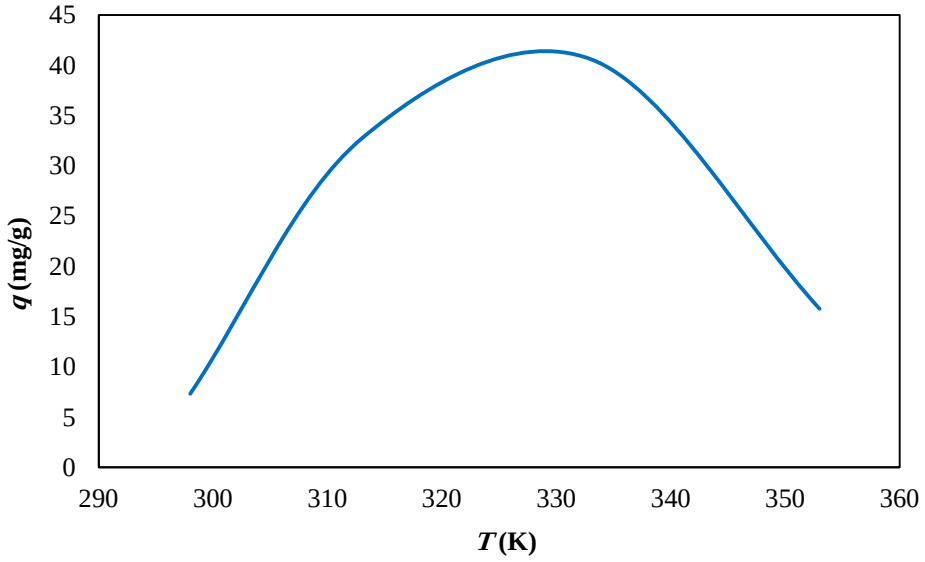

Figure 13

The variation of the amount of nitrogen adsorbed on zeolite 4A with temperature.

It seems that by increasing the temperature, the number of nitrogen molecules attaching to the surface of the adsorbent increases, so the capacity of nitrogen adsorption rises. Nevertheless, at temperatures higher than 330 K, due to the highly increased kinetic energy of nitrogen molecules, desorption happens, thereby reducing the amount of nitrogen adsorbed on zeolite 4A.

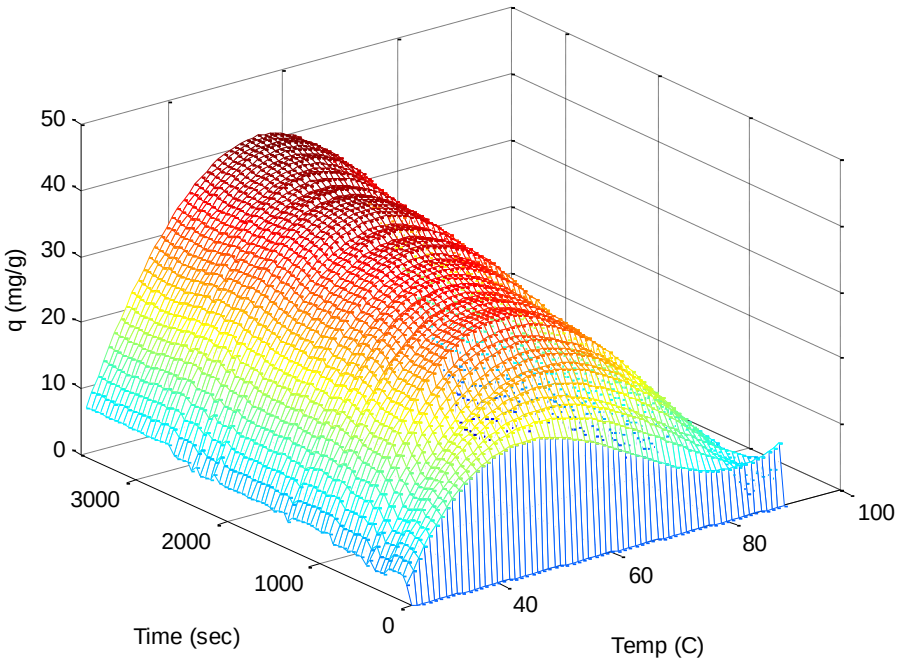

Figure 14

Three-dimensional display of the simultaneous effect of temperature and time on the capacity of nitrogen adsorption on zeolite 4A.

3.6. Effect of pressure on adsorption capacity

Figure 15 illustrates the effect of pressure on variation of the capacity of nitrogen adsorption on molecular sieve 4A versus time. One gram of molecular sieve was tested at a temperature of 298 K at four pressure values of 1, 3, 5, 7, and 9 bar. Moreover, Figure 16 depicts a three-dimensional display of the simultaneous effect of pressure and time on the capacity of nitrogen adsorption on zeolite 4A. The greatest capacity of nitrogen adsorption (376.03 mg/g) after 3600 seconds is obtained at a pressure of 9 bar, while the lowest capacity of nitrogen adsorption (6.555 mg/g) is achieved at a pressure of 1 bar. Increased pressure has a positive effect on the capacity of nitrogen adsorption. Let A be the gas adsorbed, let S equal the level of the absorbent, and let AS be the gas molecules adsorbed per unit area. By increasing pressure, according to equation $K = ([A]\,[S])/[AS]$, the adsorption capacity increased.

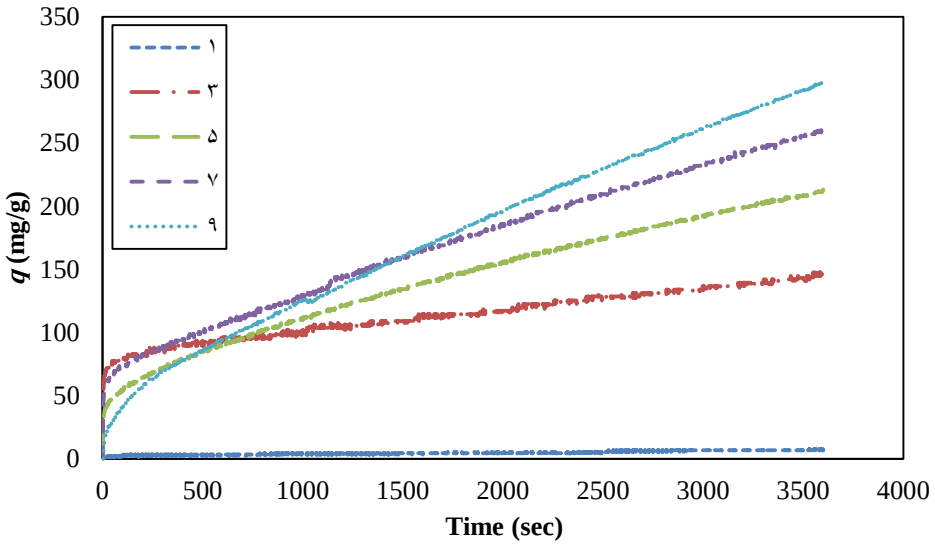

Figure 15

The variation of the capacity of nitrogen adsorption on zeolite 4A with time at different pressures.

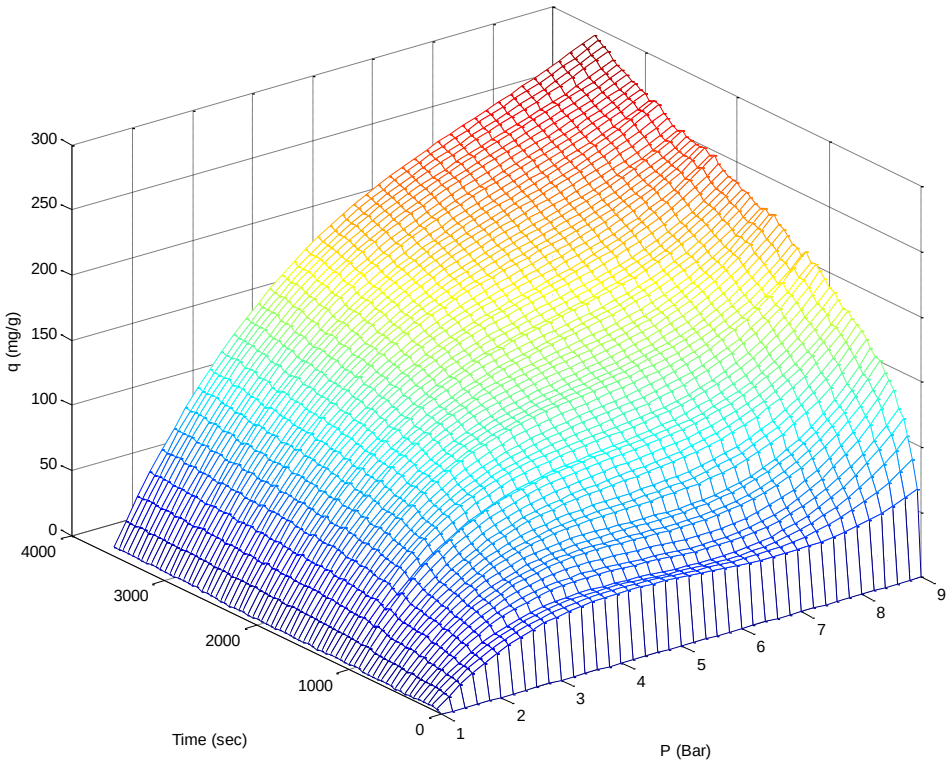

Figure 16

Three-dimensional display of the simultaneous effect of pressure and time on the capacity of nitrogen adsorption on zeolite 4A.

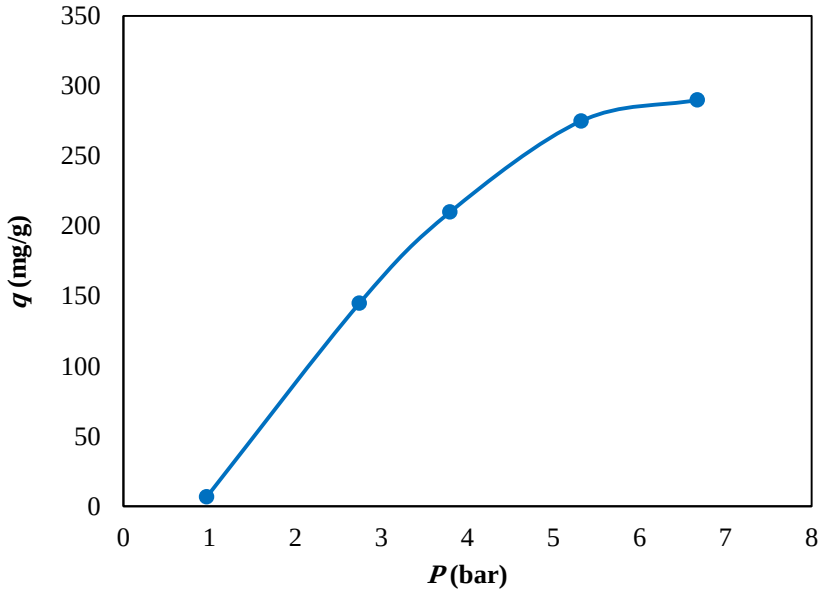

Figure 17

The variation of the amount of nitrogen adsorbed on zeolite 4A with pressure at a temperature of 298 K.

Figure 17 also demonstrates the effect of increasing pressure on the capacity of nitrogen adsorption on zeolite 4A. To this end, one gram of zeolite 4A was used at a temperature of 298 K and at different pressures of 1, 3, 5, 7, and 9 bar. The results confirm that increasing pressure raises the capacity of nitrogen adsorption on molecular sieve. At a high temperature, the effect of pressure is not accreted.

4. Conclusions

In the present work, we analyzed the effect of temperature and pressure on the capacity of nitrogen adsorption to study the equilibrium and kinetics of nitrogen adsorption on a zeolite 4A. The amount of adsorbed gas steadily increased by increasing adsorption pressure, while it first increased and then decreased by increasing the adsorption temperature. The maximum nitrogen adsorption occurred at a temperature of 333 K. Moreover, the amount of adsorbed gas decreased by raising the amount of adsorbent at a constant temperature and pressure. Finally, it can be concluded that the experimental equilibrium data on nitrogen adsorption are explained by Langmuir-Freundlich, Sips, and Koble-Corrigan models, and satisfactory results are achieved by the second order and Ritchie second order models.

Nomenclature

A	Kobel and Corrigan constant	(-)
$AARE$	Average absolute value of relative error	(-)
a_s	Sips isotherm model constant	Lg^{-1}
B	Kobel and Corrigan constant	(-)
N	Experiment number	(-)
n	Coefficient of the Freundlich	(-)
m	Mass of the adsorbent	g
$P_{N_2}^{initial}$	Nitrogen initial pressure	bar

$P_{N_2}^{final}$	Nitrogen final pressure	bar
K_L	Langmuir adsorption constant	1/bar
k_1	Constant of the Freundlich	g.bar/mmol
k_d	Distribution coefficient	cm^3/g
K_s	Sips isotherm model constant	Lg^{-1}
k_2	Second order constant	(-)
k_{id}	Rate controlling constant	$(mg/g\ s^{0.5})$
q_m	Maximum adsorption capacity	mg/g
q_e	Adsorbed at equilibrium	mg/g
qe	Adsorption capacity	mg/g
q_t	Adsorption capacity	mg/g
β_s	Heterogeneity coefficient	(-)
R^2	Correlation coefficient	(-)
$\Delta H°$	Standard enthalpy	kJ/mol
$\Delta S°$	Standard entropy	kJ/(mol.K)
R	Gas constant	kJ/(mol.K)
W	Weight of the adsorbent	g
V	Volume of the gas	cm^3

References

Ahmadi, M., Mohammadian, M., Khosravi, M. R., and Baghban, A, Experimental, Kinetic, and Thermodynamic Studies of Adsorptive Desulfurization and Denitrogenation of Model Fuels Using Novel Mesoporous Materials, Journal of Hazardous Materials, Vol. 374, p. 129-139, 2019.

Ahmadi-Pour, M., Khosravi-Nikou,M.R., and Shariati, A., Adsorption of Xylene Isomers Using Ba-faujasite Type Zeolite: Equilibrium and Kinetics Study, Chemical Engineering Research and Design, Vol. 138, p. 387-397, 2018.

Aroua, M.K., Wan Daud, W. M., Yin, Y. C., and Adinata, D., Adsorption Capacities of Carbon Dioxide, Oxygen, Nitrogen and Methane on Carbon Molecular Basket Derived from Polyethyleneimine Impregnation on Microporous Palm Shell Activated Carbon, Separation and Purification Technology, Vol. 62, p. 609-613, 2008.

Bayati, B., Ejtemaei, M., Aghdam, N. C., Babaluo, A. A., Haghighi, M., and Sharafi, A., Hydroisomerization of n-Pentane over Pt/Mordenite Catalyst: Effect of Feed Composition and Process Conditions,Iranian Journal of Oil & Gas Science and Technology, Vol. 5, p. 84-99. 2016.

Budner, Z., Dula J., Podstawa, W., and Gawdzik, A., Study and Modelling of the Vacuum Swing Adsorption (VSA) Process Employed in the Production of Oxygen, Chemical Engineering Research and Design, Vol. 77, p. 405-412, 1999.

Cheung, C., Porter, J. and McKay, G., Sorption Kinetic Analysis for the Removal of Cadmium Ions from Effluents Using Bone Char, Water Research, 35, p. 605-612, 2001.

Cussler, E.L., Diffusion: Mass Transfer in Fluid Systems, Cambridge University Press, 2009.

Chen, X., Modeling of Experimental Adsorption Isotherm Data, Information, Vol. 6, p. 14-22, 2015.

Cruz, P., Magalhães, F.D., and Mendes, A. On the Optimization of Cyclic Adsorption Separation Processes, AIChE Journal, Vol. 51, p. 1377-1395, 2005.

Delavari Amrei, H., Low-pressure Adsorption of CO_2 on Multi-wall Carbon Nanotubes, International Journal of Nanoscience and Nanotechnology, Vol. 4, p. 49-58, 2008.

Dolan, W.B., and Butwell, K.F., Selective Removal of Nitrogen from Natural Gas by Pressure Swing Adsorption, 2002, Google Patents.

Elshishini, S. S., and Elnashaie, S., Modelling, Simulation, and Optimization of Industrial Fixed Bed Catalytic Reactors, 1994.

Farooq, S., Ruthven, D.M., and Boniface, H.A., Numerical Simulation of a Pressure Swing Adsorption Oxygen Unit, Chemical Engineering Science, Vol. 44, p. 2809-2816, 1989.

Farooq, S., and Ruthven, D.M., A Comparison of Linear Driving Force and Pore Diffusion Models for A Pressure Swing Adsorption Bulk Separation Process,Chemical Engineering Science, Vol. 45, p. 107-115, 1990.

Farooq, S., and Ruthven, D.M., Numerical Simulation of a Kinetically Controlled Pressure Swing Adsorption Bulk Separation Process Based on a Diffusion Model, Chemical Engineering Science, Vol. 46, p. 2213-2224, 1991.

Fashi, F., Ghaemi, A., and Moradi, P., Piperazine-modified Activated Alumina as a Novel Promising Candidate for CO_2 Capture: Experimental and Modeling, Greenhouse Gases: Science and Technology, Vol. 9, p. 37-51, 2018.

Fernandez, G.F., and Kenney, C. N., Modeling of the Pressure Swing Air Separation Process, Chemical Engineering Science, Vol. 38, p. 827-834, 1983.

Fil, B.A., Ozmetin, C., and Korkmaz, M., Cationic Dye (Methylene Blue) Removal from Aqueous Solution by Montmorillonite, Bulletin of the Korean Chemical Society, Vol. 33, p. 3184-3190, 2012.

Hajilari, M., Shariati, A., and Khosravi-Nikou, M., Equilibrium Adsorption of Bioethanol from Aqueous Solution by Synthesized Silicalite Adsorbents, Experimental and Modeling. Adsorption, Vol. 25, p. 13-31, 2019.

Hassan, M.M., Ruthven, D.M., and Raghavan, N.S., Air Separation by Pressure Swing Adsorption on a Carbon Molecular Sieve,Chemical Engineering Science, Vol. 41, p. 1333-1343, 1986.

Ho, Y.-S., Review of Second-order Models for Adsorption Systems, Journal of Hazardous Materials, Vol. 136, p. 681-689, 2006.

Khajeh Amiri, M., Ghaemi, A., and Arjomandi, H., Experimental, Kinetics and Isotherm Modeling of Carbon Dioxide Adsorption with 13x Zeolite in a Fixed Bed Column, Iranian Journal of Chemical Engineering, Vol. 1, p. 54-64, 2019.

Koble, R.A. and Corrigan, T.E., Adsorption Isotherms for Pure Hydrocarbons, Industrial & Engineering Chemistry, Vol. 44, p. 383-387, 1952.

Khajeh, M., and Ghaemi, A., Exploiting Response Surface Methodology for Experimental Modeling and Optimization of CO_2 Adsorption onto Naoh-modified Nanoclay Montmorillonite, Journal of Environmental Chemical Engineering, Vol. 8, p. 103663, 2020.

Langmuir, I., The Constitution and Fundamental Properties of Solids and Liquids, Part I., Solids., Journal of the American Chemical Society, Vol. 38, p. 2221-2295, 1916.

Li, J., and Hitch, M., Carbon Dioxide Sorption Isotherm Study on Pristine and Acid-treated Olivine and Its Application in the Vacuum Swing Adsorption Process, Minerals, Vol. 5, p. 259-275, 2015.

Mahdizadeh, M., and Ghaemi, A., Modeling and Simulation of Chemical Adsorption of CO_2 by Polyaspartamide in a Fixed-bed Column, Nashrieh Shimi Va Mohandesi Shimi Iran (NSMSI), 2019.

Mirzaei, F., and Ghaemi, A., An Experimental Correlation for Mass Transfer Flux of CO_2 Reactive Absorption into Aqueous MEA-PZ Blended Solution, Asia-Pacific Journal of Chemical Engineering, Vol. 13, No. 6, 2018.

Mendes, A., Costa, C., and Rodrigues, A., Analysis of Nonisobaric Steps in Nonlinear Bicomponent Pressure Swing Adsorption Systems, Application to Air Separation, Industrial Engineering Chemistry Research, Vol. 39, p. 138-145, 2000.

Moghadazadeh, Z., T.J., and Mofarahi, M., Study of a Four-bed Pressure Swing Adsorption for Oxygen Separation from Air, International Journal of Chemical, Molecular, Nuclear, Materials and Metallurgical Engineering, Vol. 2, p. 140-144, 2008.

Mendes, A.M.M., Costa, C.A.V., and Rodrigues, A.R.E., Oxygen Separation from Air by PSA: Modelling and Experimental Results: Part I: Isothermal Operation. Separation and Purification Technology, Vol. 24, p. 173-188, 2001.

Qiu, H., Pan, B., Zhang, Q. J., Zhang, W. M., and Zhang,Q. X., Critical Review in Adsorption Kinetic Models, Journal of Zhejiang University-science A, Vol. 10, p. 716-724, 2009.

Rahmati, A., Ghaemi, A., and Samadfam, M., Kinetic and Thermodynamic Studies of Uranium (VI) Adsorption Using Amberlite IRA-910 Resin, Annals of Nuclear Energy, Vol. 39, p. 42-48, 2012.

Rashidi, S., Khosravi, M. R., Anvaripour, B., and Hamoule, T., Removal of Sulfur and Nitrogen Compounds from Diesel Fuel Using MSU-S, Iranian Journal of Oil & Gas Science and Technology, Vol. 4, p. 1-16, 2015

Saeidi, M., Ghaemi, A., Tahvildari, K., and Derakhshi, P., Exploiting Response Surface Methodology (RSM) As a Novel Approach for the Optimization of Carbon Dioxide Adsorption by Dry Sodium Hydroxide, Journal of The Chinese Chemical Society, Vol. 65, p. 1465-1475, 2018.

Smith, A. and Klosek, J., A Review of Air Separation Technologies and Their Integration with Energy Conversion Processes, Fuel Processing Technology, Vol. 70, p. 115-134, 2001.

Tanaka M., Ogawa Y., Miyagawa T., Watanabe T., Copolymer and Method for Producing the Same, Us Patents, US4677191A, 1987.

Umpleby, R.J. , Baxter, S.C., Chen, Y., Shah, R. N. , Shimizu, K.D., Characterization of Molecularly Imprinted Polymers with the Langmuir− Freundlich Isotherm, Analytical Chemistry, Vol. 73, No.19, p. 4584-4591, 2001.

Subha, R., and Namasivayam, C., Modeling of Adsorption Isotherms and Kinetics of 2, 4, 6-Trichlorophenol onto Microporous $ZnCl_2$ Activated Coir Pith Carbon, Journal of Environmental and Engineering Management, Vol. 18, p. 275-280, 2008.

Wang, T., and Bricker, J., Combined Temperature and Water Vapor Effects on the Lithium Hydroxide-carbon Dioxide Reaction in Underwater Life Support Systems, Environment International, Vol. 2, p. 425-430, 1979.

Yang, R.T., Gas Separation by Adsorption Processes, Butterworth-Heinemann, 2013.